FULL PAPER

ADVANCED
OPTICAL
MATERIALS

www.advopticalmat.de

Check for updates

Planarized and Compact Light Scattering Layers Based on Disordered Titania Nanopillars for Light Extraction in Organic Light Emitting Diodes

Yidenekachew J. Donie, Dominik Theobald, Somayeh Moghadamzadeh, Adrian Mertens, Ihteaz M. Hossain, Ulrich W. Paetzold, Uli Lemmer,* and Guillaume Gomard*

Dedicated to Professor Karl Leo on the occasion of his 60th birthday

In this work, the extraction of waveguided and substrate modes in organic light emitting diodes (OLEDs) is improved by using compact light scattering layers composed of a disordered 2D array of TiO_2 nanopillars. The TiO_2 nanopillars are fabricated by combining a self-assembly and a solvent-assisted lift-off process, and are further planarized by a 250 nm thin epoxy-based photoresist layer to facilitate their anode deposition and integration within the OLED stack. This fabrication route allows engineering internal light outcoupling elements with a limited amount of parasitic absorption and with easily tunable light scattering properties that are effective over a broad spectral and angular range. Taking the example of a monochromatic bottom emitting OLED (λ_{peak} = 520 nm), the authors demonstrate an efficiency enhancement of +22%$_{rel}$ upon the incorporation of the planarized light extraction layer as well as ameliorated angular emission characteristics. This approach can be integrated in a high-throughput fabrication routine and straightforwardly extended to other OLED layouts.

1. Introduction

Organic light emitting diodes (OLED) displays are nowadays mass-produced for mobile phones, tablets and TVs.[1,2] In

Y. J. Donie, D. Theobald, S. Moghadamzadeh, Dr. A. Mertens,
I. M. Hossain, Dr. U. W. Paetzold, Prof. U. Lemmer, Dr. G. Gomard
Light Technology Institute
Karlsruhe Institute of Technology
Engesserstrasse 13, 76131 Karlsruhe, Germany
E-mail: ulrich.lemmer@kit.edu; guillaume.gomard@kit.edu
S. Moghadamzadeh, Dr. A. Mertens, I. M. Hossain,
Dr. U. W. Paetzold, Prof. U. Lemmer, Dr. G. Gomard
Institute of Microstructure Technology
Karlsruhe Institute of Technology
Hermann-von-Helmholtz-Platz 1, 76344 Eggenstein-Leopoldshafen, Germany

contrast, OLED lighting is yet to be widely adopted. The latter technology is focused on niche markets: automotive and speciality lighting.[2]

Some of the critical challenges preventing the adoption of this technology for general lighting are: the cost, the efficiency, and the lifetime of the OLEDs. For example, a white OLED's lifetime is limited by its blue emitter material. This emitter consumes more power and molecularly degrades faster than the red and green emitters, which leads to an overall shorter lifespan of the device.[3,4] Consequently, a stable and a highly efficient blue emitter material is highly sought after by both high luminance OLED lighting and OLED display technology sectors.[5] A too high power consumption resulting from several optical loss channels (surface plasmon polaritons (SPP),[6,7] waveguided[8] and substrate[9,10] modes) is an additional shortcoming.[11] The SPP mode is excited upon near-field emission and propagates along the organic/metal interface. The waveguided modes refer to photons confined in the high refractive index layers (organic layers, transparent electrode). Lastly, the substrate modes denote photons trapped within the substrate due to total internal reflection at the substrate–air interface.

One possible way to improve light management while preserving the OLED layout consists in tuning the photophysical properties of the emitters to promote a horizontal orientation of the transition dipole moments.[12,13] Alternatively, or in addition, one can incorporate a light extraction element at the OLED/air interface or within the OLED stack. Thus, micro-lens arrays,[14,15] bio-inspired hierarchical structures,[16] porous polymer layers,[17–19] composite scattering films,[20,21] and surface texture[22,23] have been utilized at OLED/air interface to efficiently extract the substrate modes. Except for high refractive index substrates,[24] the waveguided modes are in this case poorly outcoupled. To outcouple both substrate and internal modes, volumetric light scattering layers[25,26] inserted between the anode and the glass substrate have proven to be efficient. This approach is based on light scattering composite films composed of a host material with embedded high/low refractive index nanoparticles. In general, these films possess a thickness ranging from a few to several tens of micrometers[25–27] and exhibit a strong haze (i.e.,

**ADVANCED
SCIENCE NEWS**

www.advancedsciencenews.com

**ADVANCED
OPTICAL
MATERIALS**

www.advopticalmat.de

fraction of diffused over overall transmitted light) together with a decrease of light transmittance of more than 17% over the visible range when compared to bare glass.[26,28] Another approach consists in processing the OLED stack directly onto a periodically nanostructured substrate.[23,29] The diffraction properties of such substrates are easily controlled, albeit optimized for a limited spectral and angular range. As a result, they lead to color-distortion effects when applied to white OLEDs. Compact light scattering layer (i.e., with a thickness of a few hundreds of nanometers) relying on disordered 2D planar nanostructures were additionally employed to allow efficient light outcoupling while maintaining stable angular and spectral emission profiles.[30–33] The devices, however, were directly processed onto such nanocorrugated substrates. This leads to local thickness inhomogeneities resulting in the degradation of its electrical properties. To mitigate this effect, the use of planarization layers applied onto the light scattering nanostructures and based on high refractive index materials ($n \approx n_{electrode}$) such as titania (TiO$_2$)[34–36] and zirconium dioxide (ZrO$_2$)[37,38] has been investigated. A key advantage of herein is the refractive index matching between the planarization layer and the transparent electrode that minimizes internal reflections and fosters the leakage of trapped waveguided modes into the light outcoupling layer.[38] However, multiple spin-coating procedures are required to fully planarize the light scattering elements with these high refractive index materials.[37]

Recently, as a method to extract internally confined light, Junhee et al.[39] reported 2D, compact scattering layers planarized with a polymer layer using a single spin coating step. The scattering layer was made of Ag nanoparticles, which strongly reduced light transmission due to parasitic absorption by the nanoparticles. To reduce parasitic absorption, Ag nanoparticles can be replaced with dielectric nanoparticles made for example of TiO$_2$, which exhibit strong light scattering cross-sections with low absorption over the visible range.

In the present study, we introduce a compact (250 nm thin) and highly transmissive internal light extraction layer with broadband and angular-stable light scattering properties that are easily controlled by the self-assembly method. Our approach is demonstrated using monochromatic (emission peak at $\lambda = 520$ nm) OLED devices, and can also be applied to white OLEDs. The design considered here consists of an internal light extraction layer based on polydisperse TiO$_2$ nanopillars (NPs) prepared by combining polymeric self-assembly and a subsequent e-beam evaporation and lift-off process. Here, structural disorder is exploited on purpose for improved optical performance. Prior to the OLED thin film layers deposition, TiO$_2$ NPs are planarized with a polymer layer that have a planar surface, high light transmittance, and whose thickness can be easily tuned. The latter properties are primarily needed to achieve efficient OLED devices with stable electrical characteristics.

In the next sections, we first introduce the self-assembly method for fabricating the TiO$_2$ NPs on glass and flexible substrates that complies with the requirements for the mass production of large-scale lighting panels. We further discuss key parameters to tune the surface morphology of the resulting TiO$_2$ NPs and analyze their optical properties. Finally, the light outcoupling efficiency of the TiO$_2$ NPs in a bottom-emitting OLED is evaluated by comparison with a device without light scattering element.

2. Results and Discussion

Light scattering TiO$_2$ NPs were fabricated by a self-assembly method (polymer blend lithography [PBL][40]) following the sequence illustrated in **Figure 1**. The PBL is based on a polymer blend consisting of two immiscible phases (polystyrene [PS] and poly(methyl methacrylate) [PMMA]) that separate on a substrate during spin coating, as shown in Figure 1a. According to our previous development for the design of light trapping reflectors in thin-film solar cells,[41] this technique yields nanostructures with a controllable degree of structural correlation. Furthermore, the surface morphology can be easily tailored by adjusting the polymer blend composition and the deposition conditions over a large substrate area, highlighting the scalability of the method.

In this study, PBL is used to generate a nanopatterned polymeric matrix with a mean height of 110 nm (see the corresponding scanning electron microscopy [SEM] images in Figure S1, Supporting Information), which is used as a temporary mask for the evaporation of the titania layer and the subsequent lift-off process. The diameter size distribution of the nanoholes in the polymer matrix covers a range of 250–780 nm to enable an efficient scattering over the whole visible spectrum. The uniformity of the nanoholes diameter and surface coverage (SC) in the polymer matrix is analyzed across a 25 cm^2 surface area (see Figure S1, Supporting Information) using SEM measurements on randomly selected spots. As shown in Figure S1, Supporting Information, the mean diameter (MD) and SC of the nanoholes is MD = 560 ± 1.75 nm and SC = 50.0 ± 0.3%. The small difference confirm that they are uniformly distributed over a few cm^2 substrate. The nanostructured polymer matrix was then coated by an electron-beam (e-beam) evaporated titania layer (measured refractive index [n] = 2.1 at $\lambda = 520$ nm), as shown in Figure 1c. Finally, the sacrificial layer (polymer matrix) was lifted-off through an ultrasonic agitated acetone bath. To facilitate the lift-off process, we limited the thickness of the deposited TiO$_2$ to 100 nm; this is within the thickness range of the polymer matrix film. To determine the SC of the resulting NPs prior to planarization, we used atomic force microscopy (AFM) as shown in **Figure 2**a–c. The SC of TiO$_2$ NPs on a glass substrate is controlled by tuning the SC of the nanopatterned polymeric matrix, as described in Experimental Section. The diameter size distribution of the TiO$_2$ NPs with highest SC (sample shown in Figure 2c) is reported in Figure 2d.

The outcoupling efficiency of the internal light extraction layer strongly relies on the refractive index contrast between the TiO$_2$ NPs structure and the planarization layer. Large refractive index contrast ensures efficient light scattering, needed for outcoupling of waveguided and substrate modes. As a result, the planarization was performed using a transparent UV-curable film (SU-8) exhibiting a refractive index $n = 1.56$ at $\lambda = 520$ nm.[42] The epoxy resin has a refractive index comparable to the glass substrate and negligible absorption at wavelengths greater than 380 nm, making it a good candidate for planarizing the TiO$_2$ NPs. From a processing view-point, the epoxy resin thickness can be easily adjusted from a few micrometers to a few hundreds of nanometers by diluting it with solvent and by varying the spin-coating parameters.[42] The planarization of 100 nm thick TiO$_2$ NPs can be seen in the focused ion
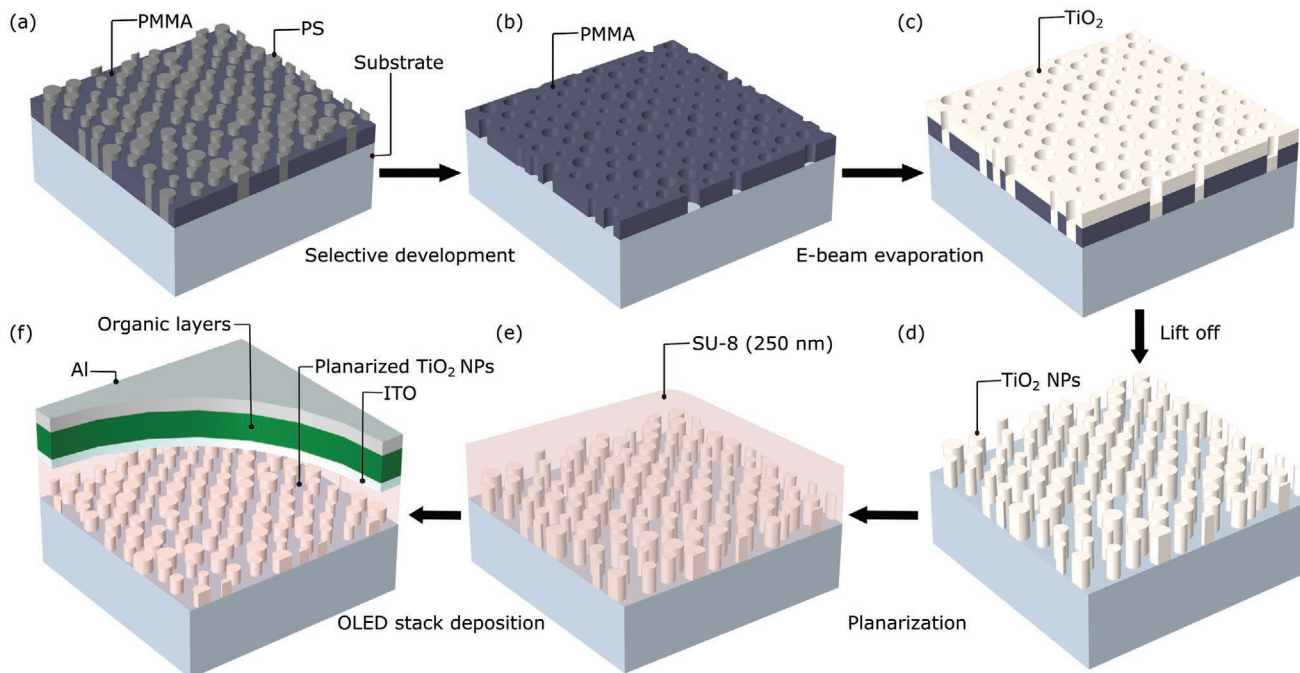
Figure 1. Schematic illustration of the fabrication process for bottom-emitting OLEDs integrating planarized TiO₂ NPs. a) Phase separation of the polymer blend, b) selective development of the PS NPs, c) e-beam evaporation of TiO₂ onto the nanopatterned PMMA matrix, d) subsequent lift-off process, and e) planarization of the TiO₂ NPs with SU-8 polymer prior to the f) deposition of a transparent and conductive oxide layer made of indium tin oxide (ITO) and an OLED stack atop.

beam (FIB)-cut cross section in Figure 2e. It is evident that the nanostructures are completely covered by the epoxy resin, which results in a planar interface that facilitates the processing of the OLED stack atop. The thickness of the planarization layer is only 250 nm, which ensures a high overlap of the wave-guided modes with the TiO₂ NPs. The FIB-cut cross section

also reveals that the vertical profile of the TiO₂ NPs is almost identical to that observed for PS NPs obtained after selective development of the PMMA phase (see Figure S2, Supporting Information). The thin line-like features at the rim of the TiO₂ NPs (see Figure 2e) most likely stem from evaporated material on the sidewalls. It does not significantly impact the optical
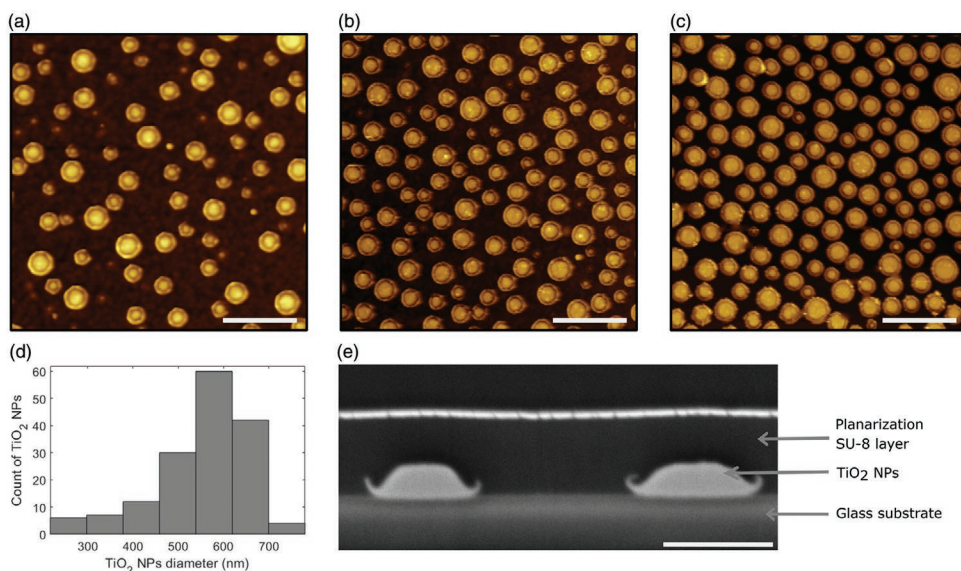
Figure 2. Topographical characterization of the internal light extraction layer. AFM images of uniformly distributed TiO₂ NPs with a mean height of 100 nm and SC of a) 19%, b) 33%, and c) 50%. The scale bar represents 2 μm. d) The diameter size distribution of the TiO₂ NPs extracted from configuration (c). e) FIB-cut SEM cross-section of planarized TiO₂ NPs. The scale bar represents 350 nm.

ADVANCED
SCIENCE NEWS
www.advancedsciencenews.com

ADVANCED
OPTICAL
MATERIALS
www.advopticalmat.de
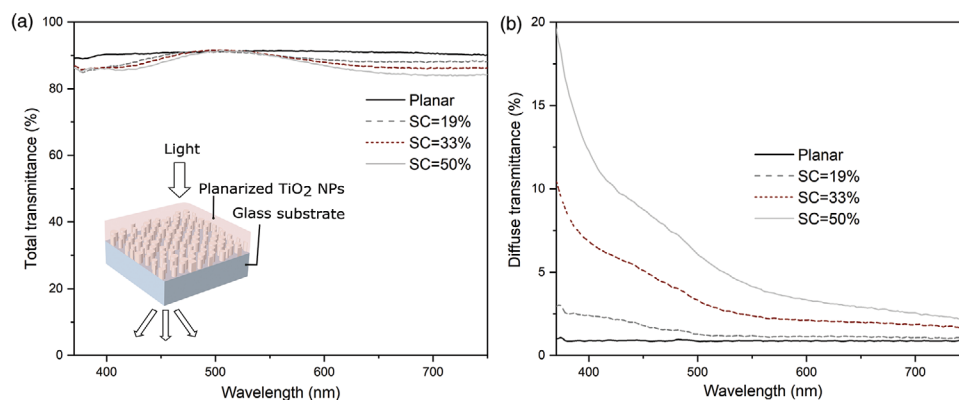
Figure 3. Measured a) total and b) diffuse transmittance with different SC of planarized TiO_2 NPs and a planar glass ("Planar") over the visible spectrum (under normal incidence). The inset depicts a scheme of the measurement setup.

properties of the scattering layer. Although demonstrated here for a glass substrate, our approach can also be used for a flexible plastic foil (see Figure S3, Supporting Information).

To assess the light scattering properties of the planarized TiO_2 NPs, we measured their overall and diffuse transmittance spectra (see also inset in **Figure 3**a). Light transmittance ranges between 90.6% and 91.1% at $\lambda = 520$ nm, that is close to the value of 91.2% measured for the reference glass substrate. This is notably higher than the values reported for dewetted

metallic (Ag) nanostructures[39] and volumetric scattering layer,[25] indicating a low parasitic absorption and low reflection (see Figure S4, Supporting Information). As reported in Figure 3b, the scattering layer with SC = 50% has the highest diffuse transmittance, which implies that the SC of the TiO_2 NPs is an important factor to reach the appropriate light scattering regime.

To demonstrate the benefits of planarized TiO_2 NPs for light management, we integrated them in monochromatic, bottom
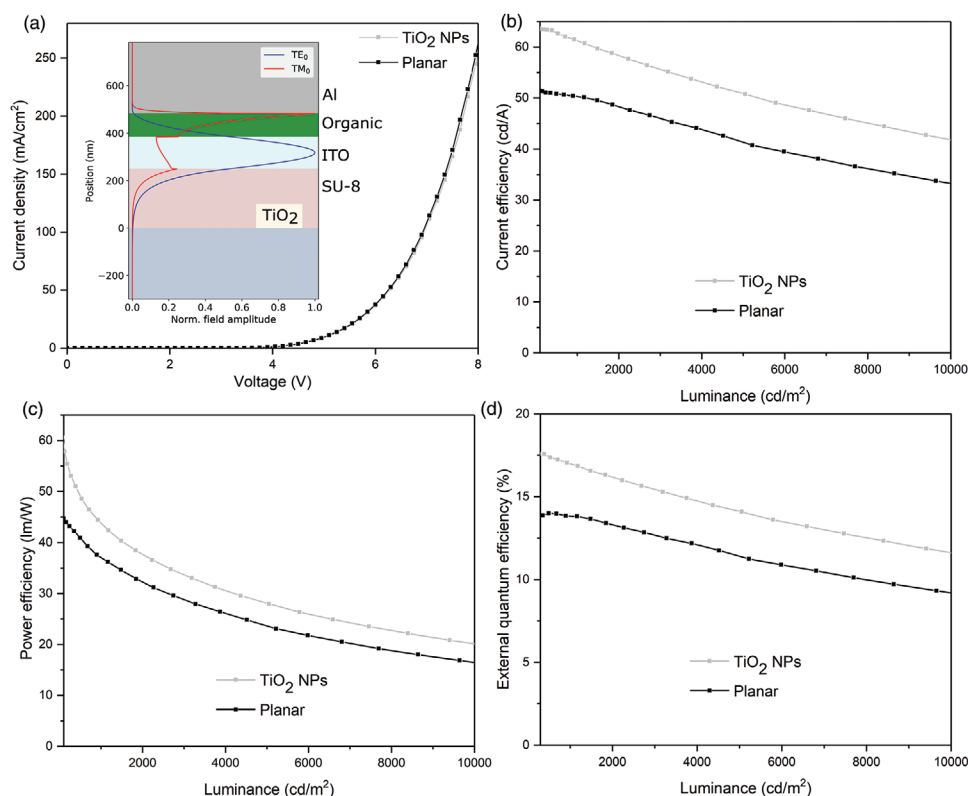
Figure 4. Electro-optical characteristics of green light emitting OLEDs without and with the compact internal light extraction layer. a) Current density–voltage characteristics with the inset showing a simulation of the mode profiles of the normalized electric field intensities in an OLED with planarized TiO_2 NPs at $\lambda = 520$ nm. b) Current, c) power, and d) external quantum efficiency (EQE) of OLEDs with and without planarized TiO_2 NPs. The SC of TiO_2 NPs is 50%. The performance data shown is that of a representative sample; however, eight OLEDs (each with a pixel area of 10 mm^2) on 25 mm × 25 mm substrates were tested and led to a similar enhancement.
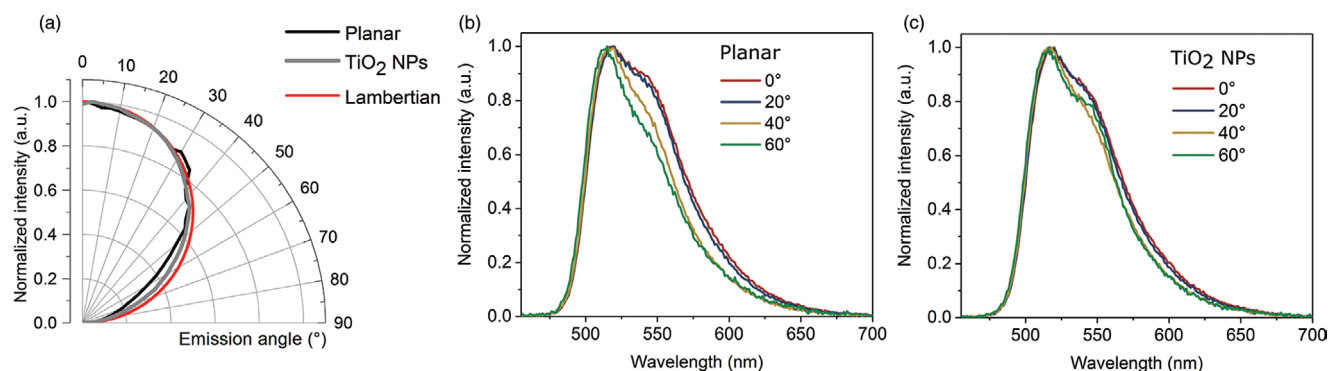
Figure 5. Emission profile of an OLED with attached macroscopic extraction hemisphere. a) Angular distribution of normalized intensity of an OLED at peak emission wavelength of 520 nm with and without planarized TiO_2 NPs. Red line represent Lambertian emission. Normalized spectra at 0°, 20°, 40°, and 60° emission angle of an OLED b) without and c) with scattering layer.

emitting OLEDs according to the layout introduced in Figure 1f. The light outcoupling capability of the planarized TiO_2 NPs was assessed by comparison to a reference device with an identical stack but without NPs fabricated on the same sputtered ITO. Owing to the planarization layer, the voltage–current characteristics of the OLEDs including the light extraction layer was found to be almost identical to the one measured for the reference planar devices as shown in **Figure 4**a. The benefit of the light extraction layer is apparent in Figure 4b–d. The planarized TiO_2 NPs allow a higher fraction of the generated light to be coupled out, as shown for the case of a SC of 50%.

The current efficiency is enhanced from 50 to 61 cd A^{-1} as shown in Figure 4b for configuration with SC = 50% at a luminance of 1000 cd m^{-2}. This corresponds to a relative increase of 22% compared to a planar reference. A similar behavior can be seen on the same plot for the power efficiency. The OLEDs with SC = 50% show an efficiency of 44 lm W^{-1}, compared to 36 lm W^{-1}, both examined at 1000 cd m^{-2}. For the configuration with SC = 33% (curves not reported here), an increase of about 10% of the current efficiency and the power efficiency is obtained. Furthermore, the configuration with SC = 19% only shows a small enhancement (4% in current efficiency and in power efficiency). The strong enhancement for the configuration with SC = 50% originates from the densely packed TiO_2 NPs (Figure 2c), and from the resulting increase of optical scattering (Figure 3b). Overall, this improved the EQE (see Figure 4d) with respect to the planar reference (EQE absolute increase of 3.3%) and outperform values reported for dewetted metallic (Ag) nanostructures[39] (EQE absolute increase of <0.5%).

Figure 5a shows the angular dependent normalized radiant intensity of OLED device with and without the planarized TiO_2 NPs. We first note that the emission profiles of the device with and without planarized TiO_2 NPs follow the angular profile of an ideal Lambertian emitter below 30°. However, the emission profile deviates from the Lambertian reference above 30° for a planar device compared to the nanostructured device. This is attributed to a weak microcavity effect.[43] The measured and normalized emission spectra shown in Figure S5, Supporting Information, and Figure 5b–c also demonstrate that the controlled amount of optical scattering can reduce the angular spectral shift observed for planar devices. The reduced viewing

angle dependence for the device with planarized TiO_2 NPs compared to the planar device supports the suitability of our light extraction layer for general lighting applications.

A continuation of this work could be dedicated to the increase in the refractive index of the planarization layer by loading the SU-8 layer with high refractive index nanoparticles. Such a planarization layer can foster the leakage of trapped light modes into the light coupling layer. Additional work could also be dedicated to increasing the height of the TiO_2 NPs. Higher light scattering NPs are known to yield better light extraction.[38,44] TiO_2 NPs with a thickness ranging from a few micrometers to a few hundreds of nanometers can be fabricated by introducing liquid cross-linkable prepolymer in the polymer blend used for the fabrication of the nanopatterned polymeric matrix, as demonstrated in ref. [45] Moreover, fully wet-processable compact light extraction layer can be achieved by infiltrating the nanopatterned polymer matrix with liquid titania precursor.

3. Conclusions

In this work, we developed an approach based on scalable polymer blend lithography to improve light management in OLEDs. This was achieved by introducing a compact light extraction layer with an overall thickness of only 250 nm, consisting of high refractive index TiO_2 NPs planarized by a transparent epoxy layer. To this end, polymer blend lithography was used to fabricate a polymeric matrix containing nanoholes serving as a lift-off mask for the subsequent fabrication of the TiO_2 NPs. This technique allows facile tuning of their morphology, including their mean diameter, density, and average inter-distance to achieve the desired light scattering properties over the visible spectrum. Moreover, the resulting structural disorder was exploited to produce an effective light extraction layer over a broad spectral range with limited angular dependency. Thus, the best planarized TiO_2 NPs configuration exhibits a mean total transmittance of 87% and a fraction of diffused transmitted light of 6% over the visible spectrum. As a proof-of-concept, the light out-coupling capability of this configuration was tested in a monochromatic bottom-emitting OLED and an efficiency enhancement of up to 22% was measured with respect to a planar device. Finally, it was shown that the

**ADVANCED
SCIENCE NEWS**
www.advancedsciencenews.com

**ADVANCED
OPTICAL
MATERIALS**
www.advopticalmat.de

introduction of planarized and controlled disordered TiO_2 NPs leads to more stable angular emission spectra that highlights the benefits of exploiting structural disorder for lighting applications. It should be noted that the developed layers can also be used to ameliorate light extraction in white OLEDs. Moreover, the scattering properties of TiO_2 NPs can be tuned across the visible and NIR spectrum by changing their structural parameters (i.e., size, inter-distance and thickness) allowing their application not only in distinct types of OLED designs but also in biosensing, solar cells, remote quantum dots thin films, head-up displays, etc.

4. Experimental Section

Fabrication of High Refractive Index Scattering Layer via Lift-Off: The PBL technique was employed to produce the polymer matrix (made of PMMA) drilled with nanoholes. Here, polymer blend solutions of PS (MW = 34 kg mol^{-1}) and PMMA (MW = 15 kg mol^{-1}) were used. PS and PMMA were purchased from Polymer Standards Service GmbH (PSS). The polymer blend solution was prepared with a PS:PMMA mass ratio of 2:8, 3:7, and 4:6. The concentration of the solution was 20 mg ml^{-1}. Each mixture of PS and PMMA was dissolved in methyl ethyl ketone (MEK, Sigma Alderich). A blend film was formed by spin coating the solutions on glass and plastic foil (poly(ethylene 2,6-naphthalate) or PEN) substrates (25 mm × 25 mm) at a speed of 800 rpm (PS: PMMA=2:8), 1000 rpm (PS: PMMA=3:7), and 1500 rpm (PS: PMMA=4:6) for 30 s. Relative humidity was maintained between 40% and 50% during spin coating. Prior to spin-coating, the substrates were cleaned in acetone and isopropanol for 10 min each. After phase separation of the polymer blends, PS was selectively developed using cyclohexane. The nanostructured polymer matrix was then coated by an electron-beam evaporated titania layer (measured n = 2.1 at λ = 520 nm). In order to obtain the TiO_2 NPs, the lift-off step was then performed by rinsing the samples with acetone for 10 min in standard ultrasonic bath. Finally, the TiO_2 NPs were covered with a 250 nm layer of SU-8 (Negative photoresist, MicroChem) for surface planarization.

Deposition of the Organic Light Emitting Film Stack: As a transparent anode material, indium tin oxide (ITO) was applied by Kurt J Lesker PVD-75 thin film deposition system. The deposition was carried out at room temperature (25 °C) with the deposition time of 2000 s, 0.8 mtorr, and 2.5% O_2. Then, the samples were further annealed for 15 min on a hot plate at 200 °C to improve the transmission and the conductivity. The layers exhibit a sheet resistance of 22.9 ohms sq^{-1} for a film thickness of 135 nm. The OLED materials were deposited using a high vacuum thermal evaporator (Lesker Spectros) at a pressure of 10^{-6} mbar. Molybdenium oxide (MoO_3) was used as a hole injection material; 4,4',4''-tris[phenyl(m-tolyl)amino]triphenylamine (m-MTDATA) as a hole transport material; tris[2-phenylpyridinato-C2, N]iridium (III) ($Ir(ppy)_3$) as the emitter material was doped in a double-layer consisting of the hole and the electron transport materials both at a concentration of 7 vol.%. As the electron transport material 4,7-diphenyl-1,10-phenanthroline (BPhen) was used followed by lithium fluoride (LiF) and aluminum (Al) as the cathode material. The OLED stack consisted of 5 nm MoO_3, 15 nm m-MTDATA, 20 nm m-MTDATA:$Ir(ppy)_3$, 20 nm BPhen:$Ir(ppy)_3$, 40 nm BPhen, 1 nm LiF, and 100 nm Al.

Topographical Investigation: The morphology of the investigated samples was probed by using atomic force microscopy (dimension icon, Veeco with NanoScope V controller) under ambient conditions in tapping mode. The cross-section view image was acquired using scanning electron microscopy (SUPRA 60 VP, Carl Zeiss Microscopy GmbH, Germany); the sample was FIB cut beforehand.

Optical Characterization: The wavelength-dependent complex optical indices of the electron-beam evaporated titania layer were determined via spectroscopic ellipsometry (WVASE system) utilizing a generalized oscillator approach. The model comprised a Cauchy layer

to account for the glass substrate and a Lorentz oscillator in order to describe the titania layer. Multiple reflections at the substrate/air interface were considered. In order to lower the parameter correlation of the fitted values, the measurement was conducted for various angles of incidences. The resulting refractive index of 2.1 at λ = 520 nm was rather low. This might be due to the amorphous nature of the titania layer, which was processed atop of a cold substrate (25 °C).[46] The total and diffused transmittances of the internal light scattering layers were measured using a UV-VIS spectrometer (Lambda 1050, PerkinElmer Inc.) equipped with a 150 mm integrating sphere. The diffused transmittance was performed by letting the direct transmittance escape out from the integrating sphere.

Characterization of the OLEDs: The electrical characteristics were measured using a source measurement unit (Keithley 2400). The luminous flux was determined by an integrating sphere attached to a spectrometer (Instrument Systems CAS140). The current efficiencies were determined assuming Lambertian emission. OLED characterization was carried out in a nitrogen atmosphere to avoid degradation of the device. The devices were encapsulated using a cavity glass attached to a UV curable resin prior to the angular emission profile. The emission profile was measured using a spectrometer (Ocean Optics USB2000+) pointing toward the sample, which was mounted on a rotating stage. The edges were blackened to block substrate mode emission.

Supporting Information

Supporting Information is available from the Wiley Online Library or from the author.

Conflict of Interest

The authors declare no conflict of interest.

[1] Y. Huang, E.-L. Hsiang, M.-Y. Deng, S.-T. Wu, *Light: Sci. Appl.* **2020**, *9*, 11.

[2] Y. Zhu, L. Guo, Y. Lee, X. Xu, J. Xie, G. Zhang, Y. Hu, in *SID Symposium Digest of Technical Papers*, Vol. *50*, Wiley Online Library, Hoboken, NJ **2019**, pp. 628–631.

[3] Z. Xu, B. Z. Tang, Y. Wang, D. Ma, *J. Mater. Chem. C* **2020**, *8*, 2614.

[4] A. Arjona-Esteban, B. Szafranowska, J. Ochsmann, in *Organic Light Emitting Diode Technology and Applications*, IntechOpen, London **2019**.

[5] T. Baumann, M. Budzinsky, in *SID Symposium Digest of Technical Papers*, Vol. 49, Wiley Online Library, Hoboken, NJ **2018**, pp. 142–144.

[6] J. Frischeisen, B. Scholz, B. Arndt, T. Schmidt, R. Gehlhaar, C. Adachi, W. Brütting, *J. Photonics Energy* **2011**, *1*, 011004.

[7] S. Wedge, W. Barnes, *Opt. Express* **2004**, *12*, 3673.

[8] K. Meerholz, D. C. Müller, *Adv. Funct. Mater.* **2001**, *11*, 251.

[9] H.-Y. Lin, J.-H. Lee, M.-K. Wei, K.-Y. Chen, S.-C. Hsu, Y.-H. Ho, C.-Y. Lin, in *Organic Light Emitting Materials and Devices XI*, *Proc. SPIE*, Vol. *6655*, International Society for Optics and Photonics, Bellingham, WA **2007**, p. 66551H.

[10] Y. Huang, Y. Liu, K. Youssef, K. Tong, Y. Tian, Q. Pei, *Adv. Optical Mater.* **2018**, *6*, 1801015.

[11] W. Brütting, J. Frischeisen, T. D. Schmidt, B. J. Scholz, C. Mayr, *Phys. Status Solidi A* **2013**, *210*, 44.

[12] T. D. Schmidt, T. Lampe, D. Sylvinson M. R., P. I. Djurovich, M. E. Thompson, W. Brütting, *Phys. Rev. Appl.* **2017**, *8*, 037001.

[13] S. Nowy, B. C. Krummacher, J. Frischeisen, N. A. Reinke, W. Brütting, *J. Appl. Phys.* **2008**, *104*, 123109.

[14] F. Galeotti, W. Mróz, G. Scavia, C. Botta, *Org. Electron.* **2013**, *14*, 212.

[15] Y. Luo, C. Wang, L. Wang, Y. Ding, L. Li, B. Wei, J. Zhang, *ACS Appl. Mater. Interfaces* **2014**, *6*, 10213.

[16] J.-J. Kim, J. Lee, S.-P. Yang, H. G. Kim, H.-S. Kweon, S. Yoo, K.-H. Jeong, *Nano Lett.* **2016**, *16*, 2994.

[17] T.-W. Koh, J. A. Spechler, K. M. Lee, C. B. Arnold, B. P. Rand, *ACS Photon.* **2015**, *2*, 1366.

[18] R. Liu, Z. Ye, J.-M. Park, M. Cai, Y. Chen, K.-M. Ho, R. Shinar, J. Shinar, *Opt. Express* **2011**, *19*, A1272.

[19] B. W. Lim, M. C. Suh, *Nanoscale* **2014**, *6*, 14446.

[20] J. Song, K.-H. Kim, E. Kim, C.-K. Moon, Y.-H. Kim, J.-J. Kim, S. Yoo, *Nat. Commun.* **2018**, *9*, 3207.

[21] K. Tong, X. Liu, F. Zhao, D. Chen, Q. Pei, *Adv. Optical Mater.* **2017**, *5*, 1700307.

[22] S. Chen, H. S. Kwok, *Opt. Express* **2010**, *18*, 37.

[23] L. Zhou, Q.-D. Ou, J.-D. Chen, S. Shen, J.-X. Tang, Y.-Q. Li, S.-T. Lee, *Sci. Rep.* **2014**, *4*, 4040.

[24] H. J. Peng, J. Y. Ho, C. Qiu, M. Wong, H. S. Kwok, in *SID Symposium Digest of Technical Papers*, Vol. 35, **2004**, p. 158.

[25] T. Eiselt, J. B. Preinfalk, K. Bittkau, G. Gomard, T. Hanemann, U. Lemmer, *Flexible Printed Electron.* **2018**, *3*, 015007.

[26] J. B. Preinfalk, T. Eiselt, T. Wehlus, V. Rohnacher, T. Hanemann, G. Gomard, U. Lemmer, *ACS Photonics* **2017**, *4*, 928.

[27] H.-W. Chang, J. Lee, S. Hofmann, Y. Hyun Kim, L. Müller-Meskamp, B. Lüssem, C.-C. Wu, K. Leo, M. C. Gather, *J. Appl. Phys.* **2013**, *113*, 204502.

[28] C.-H. Chang, K.-Y. Chang, Y.-J. Lo, S.-J. Chang, H.-H. Chang, *Org. Electron.* **2012**, *13*, 1073.

[29] J. Hauss, B. Riedel, T. Bocksrocker, S. Gleiss, K. Huska, U. Geyer, U. Lemmer, M. Gerken, in *Solid-State and Organic Lighting*, Optical Society of America, Washington, DC **2010**, p. SOThB2.

[30] Y. Li, M. Kovačič, J. Westphalen, S. Oswald, Z. Ma, C. Hänisch, P.-A. Will, L. Jiang, M. Jung haehnel, R. Scholz, S. Lenk, S. Reineke, *Nat. Commun.* **2019**, *10*, 1.

[31] R. Wang, L.-H. Xu, Y.-Q. Li, L. Zhou, C. Li, Q.-D. Ou, J.-D. Chen, S. Shen, J.-X. Tang, *Adv. Optical Mater.* **2015**, *3*, 203.

[32] B. Jiao, Y. Yu, Y. Dai, X. Hou, Z. Wu, *Opt. Express* **2015**, *23*, 4055.

[33] W. H. Koo, Y. Zhe, F. So, *Adv. Optical Mater.* **2013**, *1*, 404.

[34] C. Lee, K.-H. Han, K.-H. Kim, J.-J. Kim, *Opt. Express* **2016**, *24*, A488.

[35] C. Lee, J.-J. Kim, *Small* **2013**, *9*, 3858.

[36] J. W. Huh, J.-W. Shin, D.-H. Cho, J. Moon, C. W. Joo, S. K. Park, J. Hwang, N. S. Cho, J. Lee, J.-H. Han, H. Y. Chu, J.-I. Lee, *Nanoscale* **2014**, *6*, 10727.

[37] H. Cho, E. Kim, J. Moon, C. W. Joo, E. Kim, S. K. Park, J. Lee, B.-G. Yu, J.-I. Lee, S. Yoo, N. S. Cho, *Org. Electron.* **2017**, *46*, 139.

[38] K. Lee, J.-W. Shin, J.-H. Park, J. Lee, C. W. Joo, J.-I. Lee, D.-H. Cho, J. T. Lim, M.-C. Oh, B.-K. Ju, J. Moon, *ACS Appl. Mater. Interfaces* **2016**, *8*, 17409.

[39] J. Choi, S. Kim, C. H. Park, J. H. Kwack, C. H. Park, H. Hwang, H.-S. Im, Y. W. Park, B.-K. Ju, *ACS Appl. Mater. Interfaces* **2018**, *10*, 32373.

[40] C. Huang, M. Moosmann, J. Jin, T. Heiler, S. Walheim, T. Schimmel, *Beilstein J. Nanotechnol.* **2012**, *3*, 620.

[41] Y. J. Donie, M. Smeets, A. Egel, F. Lentz, J. B. Preinfalk, A. Mertens, V. Smirnov, U. Lemmer, K. Bittkau, G. Gomard, *Nanoscale* **2018**, *10*, 6651.

[42] K. Microchem, SU-8 2000 Data Sheet (2000.5–2015), Available at: https://kayakuam.com (accessed: September 2020).

[43] J.-W. Shin, D.-H. Cho, J. Moon, C. W. Joo, J. Lee, J. W. Huh, S. K. Park, J.-H. Han, N. S. Cho, J. Hwang, H. Y. Chu, J.-I. Lee, *Opt. Lett.* **2014**, *39*, 3527.

[44] S.-J. Park, Y. D. Kim, H. W. Lee, H. J. Yang, J.-Y. Cho, Y. K. Kim, H. Lee, *Opt. Express* **2014**, *22*, 12392.

[45] Y. Li, Y. Hao, C. Huang, X. Chen, X. Chen, Y. Cui, C. Yuan, K. Qiu, H. Ge, Y. Chen, *ACS Appl. Mater. Interfaces* **2017**, *9*, 13685.

[46] D. Mergel, D. Buschendorf, S. Eggert, R. Grammes, B. Samset, *Thin Solid Films* **2000**, *371*, 218.